Proton transfer from bisphenol-A is required to activate extranuclear-initiated estrogen receptor signaling

Regla M. Medina-Gali[1,2,3,*], Juan Martinez-Pinna[1,3,*], Reinaldo S. Dos Santos[1,2,4], Paloma Alonso-Magdalena[1,2], Marina Serrano-Maciá[1,2], Roberto Sempere-Navarro[1,2], Sergi Soriano[1,3], Georgina Fuentes-Paez[5], Lorenzo Pasquali[5], Ricardo Mallavia[1,6], Sergio Ciordia[7], Marina Grimaldi[8], Patrick Balaguer[8], Laura Marroqui[1,2] and Angel Nadal[1,2]

[1] Instituto de Investigación, Desarrollo e Innovación en Biotecnología Sanitaria de Elche (IDiBE), Universidad Miguel Hernández de Elche, Elche, Spain.

[2] CIBER de Diabetes y Enfermedades Metabólicas Asociadas (CIBERDEM), Instituto de Salud Carlos III, Madrid, Spain.

[3] Departamento de Fisiología, Genética y Microbiología, Universidad de Alicante, Alicante, Spain.

[4] Unidad de Investigación, Fundación para el Fomento de la Investigación Sanitaria y Biomédica de la Comunidad Valenciana (FISABIO), Hospital General Universitario de Elche, Elche, Alicante, Spain.

[5] Endocrine Regulatory Genomics, Department of Experimental and Health Sciences, Universitat Pompeu Fabra (UPF), Barcelona, Spain.

[6] Area of Inorganic Chemistry, Universidad Miguel Hernández de Elche, Elche, Spain.

[7] Functional Proteomics Laboratory, Centro Nacional de Biotecnología-CSIC, Madrid, Spain.

[8] Institut de Recherche en Cancérologie de Montpellier (IRCM), INSERM U1194, Université Montpellier, Institut Régional du Cancer de Montpellier (ICM), Montpellier, France.

*These authors contributed equally to this work

Corresponding author

Angel Nadal, Instituto de Investigación, Desarrollo e Innovación en Biotecnología Sanitaria de Elche (IDiBE), Universidad Miguel Hernández de Elche, 03202-Elche, Alicante, Spain.

E-mail: nadal@umh.es

ABSTRACT

Ligand binding to estrogen receptors (ERs), ERα and ERβ, controls the physiology of estrogen-responsive tissues through nuclear and extranuclear initiated pathways. We found that selective ligands activate the extranuclear pathway by a mechanism involving proton transfer. The low affinity ligand and widespread endocrine disruptor Bisphenol-A (BPA) initiated nuclear and extranuclear actions. BPA concentrations similar to the receptor affinity initiated the nuclear pathway, whereas much lower concentrations initiated the extranuclear pathway. Experiments in different cell types using deuterated molecules of BPA (d_{16}-BPA) and the ERβ agonist, diarylpropionitrile (d_2-DPN), indicated that a proton transfer from the hydroxyl groups to an amino acid acceptor within the ligand binding domain is required to activate the extranuclear pathway. Activation of the extranuclear pathway by BPA caused a rapid change in the ERβ-associated interactome that did not occur with d_{16}-BPA. To investigate this mechanism in a physiological system, we acutely injected BPA and d_{16}-BPA into male mice. BPA rapidly decreased blood glucose and increased serum C-peptide levels, whereas d_{16}-BPA had no effect. In mouse pancreatic β-cells, acute treatment with BPA closed ATP-dependent K^+

channels and increased glucose-induced insulin secretion, however d_{16}-BPA was without effect. Contrary to d_{16}-BPA, BPA modified electrical activity and increased apoptosis. RNA sequencing indicated that neither BPA nor d_{16}-BPA significantly altered gene expression. Our findings suggests that the extranuclear actions of ERs are initiated by a mechanism that requires proton transfer from ligands and may have important biological consequences. This mechanism may work for other ligands, nuclear receptors and cell types.

One Sentence Summary:

Proton-transfer from low-affinity ligands activates extranuclear Estrogen Receptor-initiated pathway

INTRODUCTION

Estrogen receptors alpha (ERα) and beta (ERβ) are involved in the regulation of many physiological processes (*1*). These receptors belong to the ligand-inducible transcription factor superfamily of nuclear receptors (*2*). They activate the so-called nuclear-initiated pathway that regulates gene transcription when the ligand-bound ER acts as a transcription factor or through the tethered mechanism, in which the ER interacts with other transcription factors, such as AP-1, Sp1 or NFκB (*3*). In addition, both ERs rapidly activate a variety of signaling cascades such as MAPK and AKT that result in downstream cellular effects, referred to as the extranuclear-initiated pathway (*4*).

The nuclear and extranuclear ER-initiated pathways elicit different patterns of physiological actions (*5-7*). This generates a medical interest to find estrogen receptor

ligands that uncouple nuclear and extranuclear ER-initiated actions to improve their pharmacological profile, avoiding unwanted effects in cancer treatment, hormone replacement therapy or others. For example, Estetrol (E4) is a natural estrogen produced in the human fetal liver during pregnancy that binds to ERα and preferentially activates the nuclear-initiated pathway (*8*). In contrast, the synthetic estrogens termed "pathway preferential estrogens" (PaPEs) bind both ERα and ERβ and preferentially activate the extranuclear-initiated ER pathway (*9*).

PaPEs retain the essential features of estrogens, such as their geometry and phenolic groups, but have a much lower affinity for the ERs. It has been proposed that a low affinity is key to selective activation of the extranuclear pathway because these low affinity ligands form an ER-ligand complex that is kinetically stable for a short time but sufficient to activate signaling pathways such as ERK or AKT. The ER-ligand complex, however, is not stable for long enough to act as a transcription factor, a process that involves a complex cascade of protein interactions which includes the recruitment of co-regulatory proteins and the activation of RNA polymerase (pol) II among others (*9, 10*).

PaPEs share some characteristics with the widespread endocrine disruptor Bisphenol-A (BPA), indeed PaPE-4 is derived from BPA and it retains its core bisphenol structure. BPA is a nonsteroidal estrogen which binds ERα and ERβ proteins but it shows about 1000-fold lower relative binding affinity than 17β-estradiol (E2) and, a potency of the transcriptional activity via the nuclear-initiated pathway between 1000 and 10000 times lower than E2 (*11, 12*). Studies published along the last two decades indicate that BPA induces effects at doses within the pico- and nanomolar range, *in vivo* (*13, 14*), *ex vivo* (*15*) and *in vitro* (*16*). Experiments using pancreatic β-cells from wild type, ERα and

ERβ knockout mice indicate that both receptors are involved in BPA actions via the extranuclear pathway at pico- and nanomolar concentrations (*17, 18*).

It is not understood why there is this mismatch between the low affinity of ERs for BPA and the high potency to elicit cell signaling. To mechanistically understand this discrepancy, we use here different deuterated BPA molecules and the ERβ-specific agonist diarylpropionitrile (DPN). Ligand deuteration is used in drug discovery to modify the efficacy and affinity of a given molecule, as the substitution of hydrogen (^{1}H) with its heavy isotope deuterium (^{2}H) produces subtle changes in the physical and chemical properties of the molecule while keeping its geometry virtually unchanged (*19, 20*). We found that the BPA-induced extranuclear effect initiated by ERβ was absent in the presence of a fully deuterated BPA (d_{16}-BPA), but remained when we used d_{14}-BPA, whose hydroxyl groups on the phenols were not deuterated. Similarly, DPN induced an ERβ-initiated extranuclear effect that was not observed in cells treated with a DPN deuterated at the two hydroxyls (d_2-DPN). According to the kinetic hydrogen isotope effect (*21*), our findings strongly suggest that the transfer of a proton from hydroxyls in ligands to an acceptor group in the binding site of the receptor is involved in activating the signaling pathway initiated by extranuclear ERβ. Experiments in mice and isolated β-cells pointed to a role for this mechanism in determining extranuclear-initiated actions in physiological systems.

RESULTS

Low-affinity ligands trigger the extranuclear-initiated pathway with high efficacy

Computational docking model shows that E2 forms hydrogen bonds in the ligand-binding pocket of ERβ with amino acids Glu^{305}, Arg^{346} and His^{475} (Fig. 1A). To study the

extranuclear-initiated pathway, we used HEK293 cells transiently transfected with a plasmid expressing human ERβ, which localized mainly outside the nucleus (Fig. S1A and S1B). Treatment with E2 during 1 hour of ERβ-transfected HEK293 cells induced phosphorylation of ERK that disappeared in cells transfected with an ERβ in which Glu^{305} was replaced by alanine (single mutant ERβ, smERβ) (Fig. 1B). We obtained the same result when the amino acids Glu^{305}/Arg^{346}/His^{475} were all replaced by alanine (triple mutant ERβ, tmERβ) (Fig. S2A).

Docking model indicates that BPA also forms hydrogen bonds with Glu^{305} and His^{475} (Fig.1A). BPA treatment during one hour increased ERK phosphorylation in HEK293 cells transfected with ERβ, producing an effect at concentrations similar to those used for E2 (Fig. 1C). Cells transfected with smERβ did not show increased ERK phosphorylation by BPA (Fig. 1C). The same results were observed in cells transfected with the tmERβ (Fig. S2B). The fact that E2 and BPA induced rapid ERK phosphorylation was not observed in the single or triple ERβ mutants, points to an essential role of these residues in the ERβ-mediated effects. It also suggests that E2 and BPA may behave as orthosteric ligands, binding to the same active site of ERβ.

To study the nuclear-initiated pathway we used the transactivation assay in HELN ERβ reporter cells (*22*). E2 activated the nuclear pathway with an EC50 of 68 pM while BPA activated the nuclear pathway with an EC50 of 351 nM (Fig. 1D). The observed affinity of the receptor population for BPA presented an IC50 of 244 nM relative to the binding of E2 (Fig. 1E).

The results described above indicate that E2 bound to ERβ with high affinity and activated both the nuclear- and extranuclear-initiated pathways with high efficacy. BPA, on the

other hand, bound to ERβ with low affinity, had a very high efficacy in activating the extranuclear-initiated pathway and a very low efficacy in activating the nuclear-initiated pathway. These differences in BPA efficacy suggest the existence of two mechanisms: one to initiate the extranuclear pathway, which barely depends on the affinity, and other to initiate the nuclear pathway, which is strongly affinity dependent.

BPA but not d_{16}-BPA induced extranuclear-initiated ERβ activation

To gain mechanistic insights into how BPA increases its efficacy in activating the extranuclear ERβ-initiated pathway, we decided to use two different deuterated BPA molecules: d_{16}-BPA, a molecule identical to BPA in which all hydrogen atoms have been exchanged for deuterium, and d_{14}-BPA, in which the exchangeable hydrogens in the phenolic oxygens are ^{1}H instead of ^{2}H. BPA, d_{16}-BPA and d_{14}-BPA were commercially available and were identified by NMR and HPLC-MS/MS (Fig. S3, Fig S4 and Fig S5). The change of ^{1}H by ^{2}H in d_{16}-BPA completely cancelled rapid BPA-induced ERK phosphorylation in HEK293 transfected with ERβ (Fig. 1F) while d_{14}-BPA had a similar effect to BPA (Fig. 1G). This indicated that the ^{1}H in the phenolic group are needed for the extranuclear pathway activation. Then, we sought to study the nuclear pathway, d_{16}-BPA presented a similar transactivation activity compared to BPA and d_{14}-BPA (Fig. 1D), and the observed binding affinity was slightly higher to that of BPA (BPA IC50=244 nM; d_{16}-BPA IC50=99 nM) (Fig. 1E). This small change in affinity could be due to altered strength of the hydrogen bonding upon deuteration, known as the Ubbelohde effect (*23*). In conclusion, the potency and efficacy of the nuclear-initiated action were identical among BPA and its two deuterated isotopologues. However, the extranuclear-initiated pathway depended on the hydroxyl groups, and their deuteration suppressed their biological effect.

The large difference we observed in the effects of d_{16}-BPA and d_{14}-BPA (Fig. 1F and G) implies a large isotope effect involving an ionization reaction, probably a proton transfer. No obvious carbon-hydrogen bond can be broken, and if the isotope effect is observed, it must be due to proton transfer from hydroxyl groups. This is supported by the fact that d_{14}-BPA, where all hydrogens except those bound to phenolic oxygens were substituted by deuterium, acted like BPA, i.e., induced ERK phosphorylation (Fig. 1G).

The different effects between d_{16}-BPA and d_{14}-BPA suggest that, although deuterium-hydrogen back-exchange occurs at the hydroxyl groups, this happens at a slow rate. To verify this experimentally, we assessed the extent to which d_{16}-BPA was transformed into d_{14}-BPA using HPLC-MS/MS in the protein-free culture medium at 1 and 24 hours. These time points were chosen to represent the exposure times used in our experimental conditions as indicated in the figures. We found that 85% and 60% of the initial d_{16}-BPA remained unchanged after dilution in culture medium for 1 and 24 hours, respectively (Fig. S6A). These results indicated that the back-exchange of ^{2}H for ^{1}H was slow in the culture medium, buffered at pH 7.4, given that BPA is slightly alkaline (BPA $pK_a = 9.6$, where K_a is the acid dissociation constant) (*24*). In fact, we would expect the pKa for d_{16}-BPA to be higher than the pKa for BPA due to the kinetic isotope effect. The higher the pK_a the slower the release of deuterium from the hydroxyls. In conclusion, the hydroxyl groups of d_{16}-BPA remained deuterated in a high proportion during the duration of the experiments.

BPA but not d_{16}-BPA induced extranuclear-initiated ERα activation

To study if the same mechanism activated the extranuclear-initiated ERα pathway, we transiently transfected HEK293 cells with a plasmid expressing human ERα. Upon transfection, more than 65% of the cells expressed ERα, which was located mostly in the nuclear or perinuclear regions (Fig. S1C and S1D). In these cells, we found that E2 and BPA increased ERK phosphorylation in a dose-dependent manner (Fig. 2A, 2B) while d_{16}-BPA did not activate ERK (Fig. 2C). Binding to ERα was identical between BPA and d_{16}-BPA (Fig. 2D) and transactivation in HELN ERα reporter cells was similar between BPA and d_{16}-BPA, although with a much lower efficacy than E2 (Fig. 2E). These experiments suggest that a similar mechanism works for the extranuclear activation of ERK by BPA binding to ERα.

DPN but not d_2-DPN induced ERβ-mediated ERK activation

To investigate if other ER ligands behave as BPA we chose the specific ERβ agonist diarylpropionitrile (DPN) (*25*) which in the docking model forms hydrogen bonds with residues Glu^{305}, Arg^{346} and His^{475} within the ERβ ligand binding domain (not shown). Experiments of competitive ligand binding performed in HELN ERβ reporter cells showed that DPN affinity for ERβ was within the low nanomolar range (IC50 = 4.3 nM) (Fig. 3A). The deuterated molecule d_2-DPN, which was synthesized by $^2H/^1H$ exchange and confirmed to have deuterated hydroxyls by HPLC-MS/MS (Fig. S6B and C), exhibited similar binding to ERβ (IC50 = 3.1 nM) (Fig. 3A). The transactivation assay demonstrated that DPN and d_2-DPN equally activated the nuclear-initiated pathway (Fig. 3B). However, only DPN induced ERK phosphorylation (Fig. 3C, 3D), while d_2-DPN did not affect it (Fig. 3E, 3F). We observed that more than 90% of d_2-DPN remained deuterated after 1 hour in culture medium (Fig. S6D) and this value dropped to nearly 50% after 24 hours (Fig. S6D). Overall, these experiments suggest that the activation of

the extranuclear-initiated ERβ pathway by DPN also involved a proton transfer mechanism.

Differential ERβ activation of extranuclear signaling pathways by E2 and BPA isotopologues

The experiments described so far strongly indicate that a proton transfer from BPA and DPN activated, with high efficacy, the ERβ-dependent phosphorylation of ERK. As this mechanism is expected to activate other extranuclear signaling pathways, we studied the interactome obtained from the co-immunoprecipitation of ERβ combined with proteomics. For these assays, HEK293 cells overexpressing ERβ were treated with E2, BPA, d_{16}-BPA and d_{14}-BPA for 1 hour. Afterwards, cell lysates were co-immunoprecipitated with an anti-ERβ antibody to identify ERβ-interacting proteins by proteomics (Fig. 4A). We identified a total of 1039 proteins and, after a screening for nonspecific binding, we selected 279 proteins interacting with ERβ. A functional pathway enrichment analysis revealed that treatment during 1 hour activated proteins directly related to ERβ involved in several signaling pathways, including ER signaling, cell cycle and cell death, and unfolding protein response (Fig. S7A and Table S1). To analyze the protein interaction pattern for each individual treatment, we performed a principal component analysis of the interacting protein profile detailed in Table S2. We found that cells treated with BPA and d_{14}-BPA presented similar populations, whereas d_{16}-BPA population was closer to vehicle-treated cells (Fig. 4B). Of note, E2-treated cells was different from BPA, d_{14}-BPA, and d_{16}-BPA populations. (Fig. 4B).

Next, we checked the abundance of proteins that co-immunoprecipitated with ERβ after the different treatments (Fig. 4C and 4D). We observed that a large number of proteins already interacted with ERβ in basal conditions (i.e., vehicle-treated cells). When we

applied E2 we observed that some of the ERβ-interacting proteins increased or decreased interaction in a similar pattern, although not identical to BPA. The d_{16}-BPA has little or no effect and its pattern is similar to that of vehicle while d_{14}-BPA presented a similar pattern to that of BPA (Fig. 4C). These data can also be plotted as a graph of the relative abundance of proteins against the different stimuli, showing how vehicle and d_{16}-BPA cluster together, and BPA clusters with d_{14}-BPA while E2 is in between (Fig. 4D).

We confirmed the results described above by measuring the expression of HPA5, CAT, JUN, ERK and CDK1 in protein lysates from cells treated with vehicle, E2, BPA d_{14}-BPA and d_{16}-BPA and co-immunoprecipitated with ERβ (Fig. 4E).

These data suggest that the ERβ activated by BPA proton transfer interacts with a large group of extranuclear proteins involved in key cellular processes.

Rapid actions of BPA and d_{16}-BPA in pancreatic β-cells

We next decided to investigate whether this proton transfer mechanism contributes to determining extranuclear signaling in a more biological setting. For this purpose, we used mouse β-cells which express ERs (*17, 26*) and are targeted by BPA. We have previously shown that acute treatment with BPA not only decreased glucose levels in mice (*27*) but also decreased ATP-dependent K^+ (K_{ATP}) channel activity and increased glucose-induced insulin secretion (GIIS) in cultured mouse β-cells (*28*).

We then treated mice with an acute injection of either BPA or d_{16}-BPA (both at 10 μg/kg) or vehicle. BPA caused a decrease in blood glucose levels at 10 and 30 minutes after the injection, whereas d_{16}-BPA did not affect glycemia (Fig. 5A and 5B). Plasma C-peptide, a valid measure of insulin secretion and indicator of pancreatic β-cell function, was measured at the same time-points. BPA injection led to higher C-peptide levels than those found in control mice, while in d_{16}-BPA a more modest increase was quantified (Fig. 5C

and 5D). No changes were observed in insulin levels (data not shown) probably due to the fact that the degradation process is much faster for insulin (half-life in humans 3–5 minutes) than that of C-peptide (half-life in humans of 20–30 minutes). It is also important to consider that C-peptide is a more reliable indicator of insulin secretion as it is not cleared by the liver (*29*).

To further study the rapid effect of BPA on insulin secretion, we measured GIIS in pancreatic islets from male mice. We observed that exposure to 1 nM BPA for 1 hour enhanced GIIS at a stimulatory glucose concentration, i.e., 11 mM, while this effect was not seen in islets treated with 1 nM d_{16}-BPA (Fig. 5E).

We have shown that acute BPA treatment decreased K_{ATP} channel activity with high efficacy in an ERβ-dependent manner, and this effect occurs within minutes, independent of gene transcription (*18, 28*). To investigate whether acute exposure to BPA or d_{16}-BPA would modulate K_{ATP} channel activity, we recorded K_{ATP} channel activity using the patch-clamp technique in the cell-attached mode in dispersed β-cells from male mice. We showed that 1 nM BPA almost completely abrogated K_{ATP} channel activity, whereas no effects were observed in d_{16}-BPA-treated-cells (Fig. 5F and 5G). Similarly, we found that DPN almost completely abolished K_{ATP} activity while d_2-DPN did not modify K_{ATP} activity (Fig. S8). These findings suggest that rapid regulation of K_{ATP} channels and GIIS in mouse β-cells, as well as serum glucose and C-peptide levels in mice by BPA involves a mechanism of proton transfer.

Longer-term consequences of acute treatment with BPA and d_{16}-BPA

To study whether the rapid actions of BPA involving proton transfer led to longer-term effects on β-cells, we exposed rat insulinoma INS-1E cells to BPA or d_{16}-BPA using two approaches: 1) cells were treated for 1 hour; after treatment, the culture medium was

removed, the cells were washed twice with PBS, and then cultured in the absence of these stimuli for 24 hours; 2) cells were treated for 24 hours and all stimuli were present throughout the experiment (Fig S9A). Transcriptomic analyses showed that BPA or d_{16}-BPA similarly modified the expression of only a few genes in both experimental approaches (Fig. 6A and Fig S9C, 9D). GIIS measurements, however, showed that 1-hour exposure to BPA decreased insulin secretion at both basal and stimulatory glucose concentrations, an effect that was not observed in d_{16}-BPA-treated cells (Fig. 6B). Conversely, in cells treated for 24 hours, both BPA and d_{16}-BPA tended to decrease GIIS, although the difference was not significant (Fig. 6C). Analysis of cell viability showed that, regardless of exposure time, only BPA induced β-cell apoptosis, whereas d_{16}-BPA had no effect (Fig. 6D). Because the β-cell is an excitable cell, we assessed its electrical activity using the perforated patch-clamp technique. Compared to vehicle-treated cells, cells exposed to BPA for 1 hour and measuring electrical activity 24 hours later, exhibited an altered action potential shape, with reductions in both the area under the action potential (~20% reduction) and the duration at half the amplitude (~25% reduction) (Fig. 6E, 6F, 6G). Treatment with d_{16}-BPA, on the other hand, only slightly decreased the area under the action potential and increased the half-width of the action potential compared to vehicle-treated cells (Fig. 6E, 6F, 6G). This modification of the action potential shape in BPA-treated cells was associated with an increase in action potential frequency during the characteristic glucose-induced action potential bursts, an effect that did not occur in cells treated with d_{16}-BPA (Fig. 6H, 6I, 6J, 6K). These findings indicate that a 1-hour BPA treatment triggers alterations in GIIS, β-cell apoptosis and electrical activity observable after 24 hours. Furthermore, it is unlikely that alterations in these β-cell parameters result from changes in gene expression. Indeed, the lack of effect of d_{16}-BPA on these β-cell features points to proton transfer from BPA as a potential mechanism.

DISCUSSION

Our results show that the endocrine disruptor BPA binds to both ERs with low affinity and, as expected, activates nuclear actions at concentrations close to its affinity constant. However, it initiates the extranuclear pathway with high efficacy, at concentrations up to 1000 times lower than its affinity. Experiments with deuterated versions of BPA and the ERβ ligand DPN, show a strong kinetic isotope effect. The greater mass of ^{2}H compared with ^{1}H results in a lower vibrational frequency and, consequently, a lower zero-point energy for the C-^{2}H or O-^{2}H bonds compared to C-^{1}H or O-^{1}H bonds. As a result, higher activation energy is required to reach the transition state for bond cleavage, leading to lower reaction rates for the deuterated analogues when the rate-determining step involves the cleavage of a covalent C-$^{1}H/^{2}H$ or O-$^{1}H/^{2}H$ bond (*20*). Thus, the lack of effect of deuterated ligands suggest that proton transfer from those ligands, specifically from phenol hydroxyls, is a mechanism for activating the extranuclear pathway. This mechanism shows a high efficacy in activating the extranuclear pathway and is less dependent on affinity compared to the mechanism that activates the nuclear pathway.

Recently synthesized PaPE ligands, including the BPA-based PaPE-4 interact with ERs to preferentially activate the extranuclear pathway. The reasoning behind is that low-affinity ligands require only the input of a triggering signal from the ER-ligand complex to initiate a kinase cascade rather than a more sustained action of the ER-ligand complex to recruit coactivators and the entire transcriptional machinery as occurs with the nuclear pathway (*9*). A similar reasoning could be applied to BPA.

It is not well understood at the molecular level how ligands, including BPA, bind to and dissociate from ERs, nor how these dynamics affect the subsequent activation of signaling

cascades. In the case of ERα ligands, it is known that the decrease in the equilibrium dissociation constant (K_D) is due to an increase in the kinetic dissociation constant (k_{off}) while the kinetic association constant (k_{on}) remains practically unchanged (*30*). Both BPA and E2 display a fast association rate constant (k_{on}=1.3x10^6 $M^{-1}s^{-1}$) and both ligands likely recognize the same conformation of the receptor (*30*). The rate of dissociation is however very different, the k_{off}= 0.27 s^{-1} for BPA and 1.2 10^{-3} s^{-1} for E2, thus BPA dissociates more rapidly than E2 giving BPA a weaker affinity for ERα (*30*). The difference in dissociation rates gives a much shorter half-life ($t_{1/2}$) of the ER-ligand complex for BPA than for E2, BPA dissociates from the receptor in seconds whereas E2 dissociates in minutes. The k_{off} is directly related with the $t_{1/2}$ of the receptor-ligand complex, $t_{1/2}=\ln 2/k_{off}$ (*31*). In the case of BPA with a k_{off}=0.27 s^{-1}, $t_{1/2}$ of the ERα-BPA complex is 2.6 s, which must be enough for a proton transfer reaction to occur. Proton transfer is one of the fastest reactions in chemistry. Activation of the GPCR, rhodopsin, which involves proton transfer reactions, occurs in a few milliseconds (*32*). Thus, the ERs-BPA complex should remain long enough for a proton transfer process to occur and trigger a conformational change that activates the extranuclear pathway.

Rapid proton transfer signaling has been demonstrated in G protein-coupled receptors (GPCRs), including rhodopsin, adrenergic and muscarinic receptors (*33-35*). Activation of rhodopsin, involves two key chemical reactions, a retinal photoisomerization and a proton transfer reaction from a retinal Schiff base to a counterion glutamate residue (*33, 36*). In this way, rhodopsin functions as a molecular off/on switch, being fully inactive in the dark and to rapidly switch to a fully active structure in the light. It is possible, therefore, that ERs function similarly in response to ligands with the appropriate chemical properties to produce proton transfer, such as BPA. After binding, the receptor will estabilize to an active conformation due to proton transfer from the ligand acting as donor

to an acceptor within the ligand binding domain. The hydroxyl groups of the ligands, BPA, DPN and E2 form H-bonds with aminoacids Glu^{305} and His^{475} in the case of ERβ and Glu^{535} or His^{524} in the case of ERα (*22*), making possible the coupling between ligands and acceptors for a ground-state proton transfer reaction (*37*). We propose that BPA and DPN activate the extranuclear-initiated ERβ signaling after a proton transfer reaction from the hydroxyls to an acceptor group, likely Glu^{305} and/or His^{475}. Thus, it is conceivable that ligand binding acts as a molecular on/off switch for extranuclear ER-mediated actions, which would explain the high efficacy of this process triggered at doses far below the K_D in the case of BPA.

Signaling proteins interacting with ERβ will respond to the active conformation "switched on" by proton transfer, initiating an array of signaling pathways involved in estrogen signaling, cell division and death, unfolding protein response, among others. Extranuclear signaling by nuclear receptors is a complex phenomenon that is less understood at the molecular level than nuclear signaling. The activation of such extranuclear pathways by ligands other than E2, such as endocrine-disrupting chemicals, has been understudied (*38, 39*). Extranuclear ER interact with a plethora of signaling proteins associated with the plasma membrane or present in the cytosol, such as G proteins and other receptors, as well as protein kinases involved in extranuclear-initiated signaling triggered by estrogens (*4*). The nuclear interactomes of activated ER are relatively well known (*40*), but the extranuclear interactome in the absence and presence of ligands is still largely undetermined. Here, we found in our interaction proteomics analyses that, in the absence of added ligands, ERβ constitutively binds to a large amount of proteins, in agreement with previous data in MCF7 cells (*41*). While the interaction map of ERβ changes similarly in the presence of BPA and d_{14}-BPA, d_{16}-BPA produced

very little change. Therefore, the overall interaction map of ERβ is likely activated by the proposed proton transfer reaction, which probably favors a conformational state responsible for activating these signaling pathways. The fact that, in addition to BPA, the ERβ-specific ligand DPN initiates the extranuclear actions through the proton transfer mechanism suggests that the natural hormone E2 could behave similarly. However, this hypothesis still needs experimental demonstration.

To investigate whether the mechanism described in HEK293 cells overexpressing ERs occurred in a more physiological system, we used β-cells because BPA directly affects β-cell biology and has diabetogenic and obesogenic effects (*42, 43*). Our *in vivo*, *ex vivo*, and *in vitro* experiments showed that following BPA treatment, *in vivo* glucose and C-peptide levels were increased, GIIS in whole islets was elevated, and K_{ATP} channel activity in isolated β-cells was decreased. In contrast, d_{16}-BPA had no effect on these parameters. Given that previous results demonstrated that both the increase in GIIS and the decrease in K_{ATP} channel activity after acute BPA treatment involved ERβ (*18, 27, 28*). The lack of effect of d_{16}-BPA might be attributed to a potential role of proton transfer from BPA upon binding to ERβ in β-cells. These results suggest that this mechanism exists in a physiological system and is involved in the regulation of β-cell function.

A brief exposure to BPA for a single hour had lasting effects on β-cell function and viability, persisting for up to 24 hours, which potentially increase the likelihood of a diabetogenic action of BPA. On the other hand, gene regulation was not significantly altered under any of the conditions tested, indicating that either there are no changes in gene expression or these changes are very small and masked by batch-to-batch variability. This raises the possibility that BPA acts through the proton transfer mechanism to activate

extranuclear ER actions and initiate signaling responses that regulate GIIS and viability, independent of gene expression. These results warrant further investigation.

Overall, our findings reported here should impact the understanding of ER function and facilitate the design of novel drugs that specifically target the nuclear and extranuclear pathways. Additionally, it should impact the identification of endocrine-disrupting chemicals, which is currently based on the shape of ligands and their interaction with receptors, primarily considering K_D, but not a chemical reaction as a molecular switch to activate ERs. Our work suggests a mechanism that does not rely exclusively on affinity to activate extranuclear ER-initiated actions and it may be extended to other ligands and nuclear receptors.

MATERIALS AND METHODS

Chemical reagents

17β-estradiol CAS number: 50-28-2 (Sigma-Aldrich, Madrid, Spain), 4,4'-(propano-2,2-diil)difenol (BPA) CAS number: 80-05-7 (Sigma-Aldrich, Madrid, Spain), d_{16}-BPA CAS number: 80-05-7 (Cambridge Isotope Laboratories, Massachusetts, USA), d_{14}-BPA CAS number: 80-05-7 (Polymer Source Inc, Canada), 2,3-bis(4-Hydroxyphenyl)-propionitrile (DPN) CAS number:1428-67-7 (Tocris, Madrid, Spain) and collagenase (Sigma-Aldrich, Madrid, Spain). Bisphenols and E2 were dissolved in DMSO (Sigma-Aldrich, Madrid, Spain).

Cell culture and transfection protocol

HEK293 cells were kindly provided by Dr. Asia Fernandez (IDiBE-UMH). Cells were cultured with Dulbecco's modified Eagle's medium (DMEM) containing 4.5 g/l glucose

and 4 mM L-glutamine (DMEM, Gibco, ref: 11965092) supplemented with 10% FBS, penicillin (100 units/ml), streptomycin (100 µg/ml) and finally incubated under humid atmosphere at 37°C in 5% CO_2. Subsequently, cells were seeded under different conditions, as required by the assay, with different treatments, using DMEM supplemented. Transfection was performed according to the supplier's instructions, using Lipofectamine 2000 reagent (Invitrogen, ref: 11668-027) and medium supplemented with 2% FBS without antibiotics. A total of 10^5 cells per well were added to 24-well plates and, after 24 hours, transfected with the following plasmids as required for the experiment: mTFP-Reporter (Rep) teal fluorescent protein plasmid, ERα plasmid (ERα), ERβ plasmid (ERβ), Triple mutant plasmid (tmERβ) or single mutant plasmid (smERβ); all at a concentration of 300 ng/well for 48 hours. Transfection efficiency was determined by western blot and immunofluorescence. After recovery time, cells were treated with the different compounds (E2, BPA, d_{14}-BPA and d_{16}-BPA) at different concentrations specified in each figure. For treatment conditions, HEK293 cells were cultured with phenol red-free DMEM (Gibco, ref: 21063029) supplemented with 5% FBS devoid of charcoal (Gibco, ref: 12676-029) during treatment.

To characterize the ERα and ERβ activities of BPA and DPN analogues, we used already established HELN hERα and HELN hERβ reporter cell lines (Grimaldi et al., 2019). Briefly, HELN hERα and HELN hERβ were obtained by stable expression of hERα and hERβ in HELN (HeLa ERE-βglobin-luciferase) cells. HELN ER cells were cultured in DMEM:Nutrient Mixture F-12 (DMEM/F-12) without phenol red and 1 g/l glucose and supplemented with 5% stripped FBS, 100 units/ml of penicillin, 100 µg/ml of streptomycin, 0.5 µg/ml puromycin and 1 mg/ml geneticin in a 5% CO2 humidified atmosphere at 37°C.

Rat insulin-producing INS-1E cells were kindly provided by Dr. C. Wollheim (Department of Cell Physiology and Metabolism, University of Geneva, Geneva, Switzerland). Cells were cultured in RPMI 1640 GlutaMAX-I, 1 mM sodium pyruvate, 10 mM HEPES, 5% fetal bovine serum, 50 µM 2-mercaptoethanol, 50 units/ml penicillin and 50 µg/ml streptomycin (*44*).

Animals, *in vivo* experiments, islet culture and dispersed islet cells

C57BL/6 male mice (9-10 weeks of age) were used. C57BL/6 mice were obtained from Envigo (C57BL/6JOlaHsd; Barcelona, Spain) for breeding by the animal experimentation service of our institution that supplied the animals for the study. Animals were kept under controlled and standardized conditions and ad libitum access to food and water. All protocols were evaluated and approved by the Animal Ethics Committee of our institution in accordance with current national and European legislation (approvals ID: UMH.IDI.AN.01.20).

For *in vivo* experiments, male mice were fasted for 6 hours and then intraperitoneal injected with a dose of glucose (1.5 g/kg body weight) followed by a vehicle, BPA (10 µg/kg body weight) or d_{16}-BPA (10 µg/kg body weight) single injection. BPA and d_{16}-BPA were dissolved in DMSO and then diluted in phosphate-buffered saline (PBS) for administration. Blood was sampled from the tail vein before, and 10 and 30 min after vehicle, BPA or d_{16}-BPA and glucose administration. Glycemia was monitored using an automatic glucometer (Accu-Chek Compact plus; Roche, Madrid, Spain) and plasma insulin and C-peptide levels were determined by ELISA (Crystal Chem, Downers Grove, IL).

Mice were euthanized by cervical dislocation and islets were isolated as previously described (*45*). For patch-clamp experiments, islets were dispersed into single cells and

plated on coverslips as previously described (*46*). Cells were maintained at 37°C in a humidified atmosphere of 95% O_2 and 5% CO_2 and 48 hours of culture were used.

Western blot assay

Cells were cultured and lysed with Laemmli buffer. Proteins were separated by SDS-PAGE and then transferred to a PVDF membrane (*26, 47*). The membranes were blocked with 5% milk, washed with TBST and incubated with primary antibodies overnight. Primary antibody used in these experiments were: ERα (ref: MA5-13191, Invitrogen, 1:1000); ERβ (ref: MA5-24807, Invitrogen, 1:1000); pERK (ref: 4370S, Cell Signalling, 1:1000); ERK total (ref: 4696S, Cell Signalling, 1:2000); β-actin (ref: 5316, Sigma, 1:5000); GAPDH (ref: 5174, Cell signalling, 1:1000) The membranes were then washed three times with TBS-T, and incubated with secondary antibodies for 1 h. The secondary antibodies used were: Goat Anti-mouse (ref: 1706516, BIORAD, 1:5000) or Goat Anti-rabbit (ref: 1706515, BIORAD, 1:5000). The membranes were incubated with SuperSignal West Femto chemiluminescent substrate (Thermo Fisher Scientific, ref: 34096), and the protein bands were detected and visualised using a transilluminator kit (Bio-Rad, Hercules, CA, USA). The intensities of the bands were quantified by scanning densitometry (Un-SCAN software, MA, USA).

Synthesis of d_2-DPN

The synthesis of d_2-DPN was carried out from commercial DPN. First, DPN obtained from TOCRIS (Bristol, UK; Ref: 1494) was dissolved in deuterated DMSO (SIGMA-Merck, Ref: 103591) with 0.1 equivalent of HCl. Deuterium were introduced through a reaction with D_2O at 50°C and sonication for 25 minutes. After this time, samples were kept in a hot bath for 2 hours at 80ºC and finally, the samples were lyophilised and dry stored until use.

Determination of BPA and DPN isotopologues by HPLC-MS/MS

Liquid chromatography LC-MS/MS equipped with a diode array detector (DAD) and coupled to a triple quadrupole mass spectrometer Shimadzu LCMS-8050 were used to analyse the samples of interest. Samples (10 µl) were injected through an autosampler, separated on an Agilent Zorbax ODS column (150 mm × 3 mm, 5 µm) at 30°C and detected by DAD (UV 214 nm). The flow rate was set at 0.3 ml /min with methanol and water as mobile phase. The linear gradient started isocratic at 50% methanol for 3 min, then increased to 90% in 7 min and 100% in another 8 min and was maintained for another 2 min, then the gradient returned to 50% methanol in 2 min and was maintained for 5 min. The mass spectrometer was operated in ESI-negative mode, using multiple reaction monitoring mode for quantification. Nitrogen was used as a cover gas and auxiliary gas. The gas temperature was 350°C, the nebuliser was 40 psi, the gas flow was 10 l/min, and the capillary was 4500 V. Data were analysed using Qualitative Analysis B.06.00 software (Agilent, CA, USA) (*48*).

Identification of BPA isotopologues by NMR

^{1}H-NMR spectra were recorded on a Bruker AVANCE 500 spectrometer Bruker AC-300, ARX-300 and AV-400 instruments. Chemical shifts (δ) are reported in ppm and referenced to d_6-DMSO (2.50 ppm) (*49*). All of the NMR spectra were recorded in d_6-DMSO at 293 K.

GIIS assays

GIIS in mouse islets and INS-1E cells was performed as previously described (*18, 50*). After isolation, islets were allowed to recover for 2 hours. Afterwards, islets (5 islets/group) were transferred to a Krebs-Ringer buffer without glucose ("Starvation"). After a 2-hour starvation period, DMSO (Vehicle), 1 nM BPA, or 1 nM d_{16}-BPA was added to each glucose solution (2.8 or 11 mM) so that islets remained under treatment

throughout the entire assay (1-hour exposure). For INS-1E cells, after a 2-hour starvation period in Krebs-Ringer buffer without glucose, the cells were stimulated with either 1.7 mM or 17 mM glucose for 30 minutes in the absence of treatments. For whole islets and INS-1E cells, after each stimulatory period, the incubation medium was collected, placed on ice, and centrifuged at 1,400 g for 5 minutes at 4 °C. The supernatant was then transferred into a fresh tube and stored at -80°C until needed for insulin measurements. Insulin levels were measured using a mouse or rat insulin ELISA kit (Mercodia, Uppsala, Sweden).

Patch Clamp recordings

K_{ATP} channel activity was recorded using standard patch-clamp recording procedures from isolated β-cells as described previously (*46, 51*). Around 80–90% of the single cells were identified as β-cells by their response to high glucose, consisting in action currents in the cell-attached configuration. Currents were recorded using an Axopatch 200B patch-clamp amplifier (Molecular Devices LLC, CA, USA). Patch pipettes were pulled from borosilicate capillaries (Sutter Instruments Co. CA, USA) using a flaming/brown micropipette puller P-97 (Sutter Instruments Co. CA, USA) with resistance 3-5 MΩ when filled with the pipette solutions as specified below. Bath solution contained (in mM): 5 KCl, 135 NaCl, 2.5 CaCl2, 10 HEPES and 1.1 MgCl2 (pH 7.4) and supplemented with glucose as indicated. The pipette solution contained (in mM): 140 KCl, 1 MgCl2, 10 HEPES and 1 EGTA (pH 7.2). The pipette potential was held at 0 mV throughout recording. K_{ATP} channel activity was quantified by digitizing 60 s sections of the current record, filtered at 1 kHz, sampled at 10 kHz by a Digidata 1550B (Molecular Devices LLC,. CA, USA), and calculating the mean open probability of the channel (NP_o) during the sweep. Channel activity was defined as the product of N, the number of functional channels, and P_o, the open-state probability. P_o was determined by dividing the total time

channels spent in the open state by the total sample time. The recordings of the electrical activity were performed with the perforated-patch configuration and the bath solution contained (in mM): 140 NaCl, 3.6 KCl, 1.5 CaCl2, 0.5 MgCl2, 10 HEPES and 0–11 glucose (pH 7.4 with NaOH) and the pipette solution consisted of (in mM) 76 K2SO4, 10 KCl, 10 NaCl, 1 MgCl2 and 5 HEPES (pH 7.35 with KOH). Amphotericin B (120–240 μg/ml; Sigma) was added to the pipette solution to perforate the patch. The series resistance of the pipette usually increased to 20–30 MΩ after amphotericin-B perforation. Potential values were not corrected for the liquid junction potential. Data were filtered (1 kHz) and digitized (10 kHz) using a Digidata 1550B (Molecular Devices LLC, CA, USA) and stored in a computer for subsequent analysis using commercial software (pClamp11, Molecular Devices LLC, CA, USA). All experiments were carried out at 36 °C.

Assessment of cell viability

The percentages of live, apoptotic, and necrotic cells were assessed using DNA-binding dyes Hoechst 33342 and propidium iodide, following a previously established protocol (*52*). To minimize bias, two independent observers, with one blinded to the sample identities, counted at least 500 cells per experimental condition (the agreement between observers was over 90%). The results are presented as the percentage of apoptotic cells.

Transactivation assays

The cells were seeded in white 96 well plates (Greiner CellStar) with a density of 25,000 cells per well in assay growth media. Cells were incubated for 24 h at 37°C and 5% CO2, then the media was decanted and replaced with the sample serially diluted in phenol red free DMEM/F-12 with 5% dextran coated charcoal stripped FBS and 1% penicillin/streptomycin. The maximum solvent concentration was 0.1%. Samples were incubated for a further 16 h to 24 h at 37°C at 5% CO2. After the exposure period, the

test media was decanted and replaced with test media containing 0.3 mM luciferin. Luminescence, expressed as relative light units (RLU), was measured using a PerkinElmer MicroBeta luminometer. All samples were run in quadruplicate per plate and were run in at least two independent experiments.

Competitive binding assays

HELN ERα and HELN ERβ cells were seeded in white 96 well plates with clear bottom (Greiner CellStar) with a density of 75,000 cells per well in assay growth media. The cells were incubated for 24 h at 37°C and 5% CO2, then the media was decanted and replaced with the sample serially diluted in the media and tritiated reference ligand (0.1 nM E2). The maximum solvent concentration was 0.1%. The samples were incubated for a further 2 h at 37°C at 5% CO2. After the exposure period, unbound material was aspirated and the cells were washed three times with cold PBS. After visual inspection to check the good condition of the cells, 100 μL of LSC cocktail (Emulsifier-Safe, Packard Bioscience) were added and plates were agitated for 5 min. Bound radioactivity values were expressed in disintegrations per minute (dpm). Results were plotted as the percentage of radioactivity (in dpm) versus the concentration of the unlabeled reference compound (M) or water samples. All samples were run in quadruplicate per plate and were run in at least two independent experiments.

Immunofluorescence assay

HEK293 cells transfected with ERα or ERβ as appropriate were fixed with 4% paraformaldehyde (SIGMA, ref: 1635) in PBS for 15 min, then permeabilised with 0.2% Triton X-100 (Sigma, Ref: T8787) for 10 min and blocked with 5% BSA (CAPRICORN, Cat: BSA-1T) in PBS for 1 hr. Antibodies for rabbit ERα (Invitrogen, Ref: MA5-14501, 1:200) and mouse ERβ (Thermo Fisher Scientific, ref: MA1-23217, 1:200) were used,

followed by secondary anti-rabbit Alexa Flour 488 (Thermo Fisher Scientific, ref: A32723, 1:1000) and anti-mouse Alexa fluor 567 (Thermo Fisher Scientific, ref: A32740, 1:1000) antibodies. As negative controls, the samples were incubated with the secondary antibodies without primary antibodies. Finally, the nuclei of the cells were stained with DAPI (SIGMA, ref: DUO82040). Cells were observed using a Zeiss Confocal LSM900 microscope equipped with a camera (Zeiss-Vision, Munich, Germany), and images were acquired at x63 magnification and analysed using ZEN software (version 3.2; Zeiss-Vision, Munich, Germany).

Co-immunoprecipitation assay.

Immunoprecipitation was performed according to the protocol described previously (*26*). HEK293 cells were seeded in 6-well plates at a density of 10^6 cells/well and transfected with 2 µg of ERβ plasmid and were treated with different compounds (Vehicle, E2, BPA, d_{14}-BPA and d_{16}-BPA) at the concentration of 1 nM for 1 hour. After treatment, HEK293 cells were lysed with immunoprecipitation buffer (50 mM Tris, pH 7.5, 4 mM NaCl, 2 mM $MgCl_2$, 10 mM NaF, 1 mM PMSF, 1% Triton X-100 and Complete Protease inhibitor mixture, Roche Diagnostics) for 45 min on ice and centrifuged at 20,000 g for 10 min at 4ºC. They were then cleaned with Protein-G-Dynabeads magnetic beads (Thermo Fisher Scientific, Cat. No 53139) for 1 h at 4°C to remove non-specific binding proteins. After removal of the protein-G beads, the same amount of protein lysates was incubated with antibodies for ERβ (Invitrogen, Ref: MA5-24807), overnight, while mouse IgG (Cell signalling, Ref: 2729S) was used as a negative control. After incubation, immunoprecipitated were washed and resuspended with Laemmli buffer. The immunoprecipitated proteins were analysed by proteomics and western blotting.

The antibodies used in western blots of this experiment were: HSPA5 (ref: PA1-014A, Invitrogen, Massachusetts, USA, 1:1000); CAT (ref: 12980S, Cell Signalling, 1:1000),

CDK1 (ref: ab133327, Abcam, 1:1000); JUN (ref: 9165S, Cell Signalling, 1:1000); ERK (ref: 4696S, cell Signalling, 1:2000); IGG (ref: 2729S, Cell Signalling, 1:5000).

S-Trap™ digestion for proteomics

Each sample was diluted with lysis buffer to 5% sodium dodecyl sulfate (SDS) and 25 mM triethylammonium bicarbonate (TEAB). Samples were reduced and alkylated by adding 5 mM tris(2-carboxyethyl)phosphine (TCEP) and 10 mM chloroacetamide (CAA) for 30 minutes at 60ºC.

Protein digestion in the S-Trap filter (Protifi, Huntington, NY, USA) was performed following the manufacturer's instructions with minor changes (*53*). Each sample was digested at 37°C overnight using a trypsin:protein ratio of 1:15 and was cleaned with a StageTip C18 prior to LC-ESI-MS/MS analysis.

Liquid chromatography and mass spectrometry analysis (LC-ESI-MS/MS) for proteomics

After desalting, peptide concentration was measured by Qubit™ Fluorometric Quantitation (Thermo Fisher Scientific). Half of each digested sample was subjected to 1D-nano LC ESI-MS/MS (Liquid Chromatography Electrospray Ionization Tandem Mass Spectrometric) analysis using an Ultimate 3000 nano HPLC system (Thermo Fisher Scientific) coupled online to a Orbitrap Exploris 240 mass spectrometer (Thermo Fisher Scientific). Peptides were eluted onto a 50 cm × 75 µm Easy-spray PepMap C18 analytical column at 45°C and were separated at a flow rate of 250 nL/min using a 90 min gradient ranging from 2 % to 95 % mobile phase B (mobile phase A: 0.1% formic acid (FA); mobile phase B: 100 % acetonitrile (ACN), 0.1 % FA).

Data acquisition was performed using a data-dependent top-20 method, in full-scan positive mode, scanning 350 to 1200 m/z. Survey scans were acquired at a resolution of

60,000 at m/z 200, with Normalized Automatic Gain Control (AGC) target (%) of 300 and a maximum injection time (IT) of 40 ms. The top 20 most intense ions from each MS1 scan were selected and fragmented via Higher-energy collisional dissociation (HCD). Resolution for HCD spectra was set to 45,000 at m/z 200, with AGC target of 200 and maximum ion injection time of 120 ms. Isolation of precursors was performed with a window of 1 m/z, exclusion duration (s) of 10 and the HCD collision energy was 32. Precursor ions with single, unassigned, or six and higher charge states from fragmentation selection were excluded.

Proteomics data analysis and sequence search

Raw instrument files were processed using Proteome Discoverer (PD) version 2.5.0.400 (Thermo Fisher Scientific). MS2 spectra were searched using Mascot Server v2.8.0 (Matrix Science, London, UK) and a target/decoy database built from sequences in the Homo sapiens proteome at Uniprot Knowledgebase (20230420). All searches were configured with dynamic modifications for pyrrolidone from Q (-17.027 Da) and oxidation of methionine residues (+15.9949 Da) and static modification as carbamidomethyl (+57.021 Da) on cysteine, monoisotopic masses, and trypsin cleavage (max 2 missed cleavages). The peptide precursor mass tolerance was 10 ppm, and MS/MS tolerance was 0.02 Da. The false discovery rate (FDR) for proteins, peptides, and peptide spectral matches (PSMs) peptides was kept at 1%.

Pathways enrichment analysis

Enrichment pathway analysis was performed using Cytoscape version 3.9.1 with ClueGO version 2.5.9 (*54*) and CluePedia version 1.5.0 (*55*) plugins. GO Biological Process databases were used and those with a P-value <=0.05 were considered as threshold values. The model organism Homo sapiens was used for ClueGO analyses. Principal component

analysis (PCA) and clustering of relative protein abundance by treatment were performed using ClustVis software (https://biit.cs. ut.ee/clustvis/) (*56*).

Molecular modelling

Structures available in the Protein Data Bank have been used for both human LBD-ERα and ERβ, where the protein and E2 or BPA are co-crystallized, 2OCF, 3UU7 and 5TOA, respectively. These structures contained unresolved residues in mobile regions of the protein that diffracted poorly, the missing amino acids were reconstructed after generation of a homology model in the Swiss-Model server (*57*). In addition, a molecular docking technique was performed to generate the structure of LBD-ERβ with BPA within the LBD cavity, using YASARA Structure v22.5.22 software (*18, 26*). The ligand-protein interactions have been detected with the Protein-Ligand Interaction Profiler (FLIP) algorithm (*58*). The figure has been prepared with PyMol Software (Schrödinger, L. & DeLano, W., 2020. PyMOL, Available at: http://www.pymol.org/pymol).

RNA-seq processing

Raw fastq files were processed using the nf-core/rnaseq pipeline version (3.11.1) with default parameters implemented in Nextflow v23.04.2. In short, reads were trimmed using trimGalore! (https://www.bioinformatics.babraham.ac.uk/projects/trim_galore/), aligned to the rat reference genome RGSC 6.0 (rn6) release using STAR (*59*) and quantified by Salmon (*60*). The results were then loaded into R using tximport (*61*) (version 1.26.0) and the transcript information was summarized into gene annotations. Only protein-coding genes located in autosomes were retained for downstream analysis.

Differential analysis of RNA-seq

The output of Salmon was used as the input matrix for downstream analysis. The generated matrices were normalized and differential analysis was performed using

DESeq2 v.1.38.3 (*62*) using default parameters. Genes were considered significantly upregulated (gained) when adjusted p-value < 0.05 and $\log_2$ fold change > 1 and significantly downregulated (lost) when adjusted p-value < 0.05 and $\log_2$ fold change < -1. All genes that did not pass these thresholds were classified as stable/equally regulated. Moreover, in order to remove sources of potential unwanted variation, we estimated the surrogate variables using sva (*63*) and, when computing the differential analyses, we used them as covariates to fit the model.

Statistical analysis

The GraphPad Prism 8.0 software (GraphPad Sofware, Inc., CA, USA) was used for all statistical analyses. Detailed information on the statistical analysis performed in each case, including replicates, as well as the number of times the experiments were repeated, is given in the figure legends. Data are expressed as mean±SEM. To assess differences between working groups, paired t-test, one-way or two-way analysis of variance (ANOVA) was used where appropriate. A probability level ≤0.05 was considered statistically significant. P-values are indicated in the text or in the figure legends.

Supplementary Materials

[Present a list of the titles of the Supplementary Materials, in the following order: Supplementary materials and methods, supplementary figures, supplementary tables, other supplementary files, such as movies, data, interactive images, or database files. Be sure to submit all Supplementary Materials with the manuscript.]

Materials and Methods
Fig. S1. Title of the first supplementary figure.
Fig. S2. Title of the second supplementary figure.
Table S1. Title of the first supplementary table.
Data file S1. Title of the first supplementary data file.
Movie S1. Title of the first supplementary movie.

Fig. S1: Immunocytochemistry of ERα and ERβ in HEK293 cells.
Fig. S2. E2 and BPA had no effect on mutant ERβ and not transfected cells.
Fig. S3. Chemical characterization of BPA.
Fig. S4. Chemical characterization of d_{14}-BPA.

Fig. S5. Chemical characterization of d_{16}-BPA.
Fig. S6. Chemical characterization of DPN.
Fig. S7. Interactome analysis.
Fig. S8. DPN action on K_{ATP} channel activity.
Fig. S9. Transcriptome analysis.
Table S1. Functional pathways overrepresented in the interactome of HEK293 cells transiently transfected with ERβ.
Table S2. ERβ interactome.

REFERENCES AND NOTES

1. C. J. Gruber, W. Tschugguel, C. Schneeberger, J. C. Huber, Production and actions of estrogens. *N Engl J Med* **346**, 340-352 (2002).
2. J. M. Hall, D. P. McDonnell, Coregulators in nuclear estrogen receptor action: from concept to therapeutic targeting. *Mol Interv* **5**, 343-357 (2005).
3. P. Ascenzi, A. Bocedi, M. Marino, Structure-function relationship of estrogen receptor alpha and beta: impact on human health. *Mol Aspects Med* **27**, 299-402 (2006).
4. E. R. Levin, S. R. Hammes, Nuclear receptors outside the nucleus: extranuclear signalling by steroid receptors. *Nat Rev Mol Cell Biol* **17**, 783-797 (2016).
5. A. Pedram *et al.*, Developmental phenotype of a membrane only estrogen receptor alpha (MOER) mouse. *J Biol Chem* **284**, 3488-3495 (2009).
6. A. Pedram *et al.*, Estrogen reduces lipid content in the liver exclusively from membrane receptor signaling. *Sci Signal* **6**, ra36 (2013).
7. M. Adlanmerini *et al.*, Mutation of the palmitoylation site of estrogen receptor alpha in vivo reveals tissue-specific roles for membrane versus nuclear actions. *Proc Natl Acad Sci U S A* **111**, E283-290 (2014).
8. A. Abot *et al.*, The uterine and vascular actions of estetrol delineate a distinctive profile of estrogen receptor alpha modulation, uncoupling nuclear and membrane activation. *EMBO Mol Med* **6**, 1328-1346 (2014).
9. Z. Madak-Erdogan *et al.*, Design of pathway preferential estrogens that provide beneficial metabolic and vascular effects without stimulating reproductive tissues. *Sci Signal* **9**, ra53 (2016).
10. P. Yi *et al.*, Structural and Functional Impacts of ER Coactivator Sequential Recruitment. *Mol Cell* **67**, 733-743 e734 (2017).
11. G. G. Kuiper *et al.*, Interaction of estrogenic chemicals and phytoestrogens with estrogen receptor beta. *Endocrinology* **139**, 4252-4263 (1998).
12. J. M. Molina-Molina *et al.*, In vitro study on the agonistic and antagonistic activities of bisphenol-S and other bisphenol-A congeners and derivatives via nuclear receptors. *Toxicol Appl Pharmacol* **272**, 127-136 (2013).
13. L. N. Vandenberg, C. M. Schaeberle, B. S. Rubin, C. Sonnenschein, A. M. Soto, The male mammary gland: a target for the xenoestrogen bisphenol A. *Reprod Toxicol* **37**, 15-23 (2013).
14. M. Susiarjo, T. J. Hassold, E. Freeman, P. A. Hunt, Bisphenol A exposure in utero disrupts early oogenesis in the mouse. *PLoS Genet* **3**, e5 (2007).
15. L. Speroni *et al.*, New insights into fetal mammary gland morphogenesis: differential effects of natural and environmental estrogens. *Sci Rep* **7**, 40806 (2017).
16. Y. J. Jeng, C. S. Watson, Combinations of physiologic estrogens with xenoestrogens alter ERK phosphorylation profiles in rat pituitary cells. *Environ Health Perspect* **119**, 104-112 (2011).
17. P. Alonso-Magdalena *et al.*, Pancreatic insulin content regulation by the estrogen receptor ER alpha. *PLoS One* **3**, e2069 (2008).

18. L. Marroqui *et al.*, Bisphenol-S and Bisphenol-F alter mouse pancreatic beta-cell ion channel expression and activity and insulin release through an estrogen receptor ERbeta mediated pathway. *Chemosphere* **265**, 129051 (2021).
19. R. M. C. Di Martino, B. D. Maxwell, T. Pirali, Deuterium in drug discovery: progress, opportunities and challenges. *Nat Rev Drug Discov* **22**, 562-584 (2023).
20. J. Atzrodt, V. Derdau, W. J. Kerr, M. Reid, Deuterium- and Tritium-Labelled Compounds: Applications in the Life Sciences. *Angew Chem Int Ed Engl* **57**, 1758-1784 (2018).
21. F. H. Westheimer, The Magnitude of the Primary Kinetic Isotope Effect for Compounds of Hydrogen and Deuterium. *Chemical Reviews* **61**, 265-273 (1961).
22. V. Delfosse *et al.*, Structural and mechanistic insights into bisphenols action provide guidelines for risk assessment and discovery of bisphenol A substitutes. *Proc Natl Acad Sci U S A* **109**, 14930-14935 (2012).
23. M. Krzan, J. Keuschler, J. Mavri, R. Vianello, Relevance of Hydrogen Bonds for the Histamine H2 Receptor-Ligand Interactions: A Lesson from Deuteration. *Biomolecules* **10**, (2020).
24. G. Zeng *et al.*, Adsorption behavior of bisphenol A on sediments in Xiangjiang River, Central-south China. *Chemosphere* **65**, 1490-1499 (2006).
25. M. J. Meyers *et al.*, Estrogen receptor-beta potency-selective ligands: structure-activity relationship studies of diarylpropionitriles and their acetylene and polar analogues. *J Med Chem* **44**, 4230-4251 (2001).
26. I. Babiloni-Chust *et al.*, G protein-coupled estrogen receptor activation by bisphenol-A disrupts the protection from apoptosis conferred by the estrogen receptors ERalpha and ERbeta in pancreatic beta cells. *Environ Int* **164**, 107250 (2022).
27. P. Alonso-Magdalena, S. Morimoto, C. Ripoll, E. Fuentes, A. Nadal, The estrogenic effect of bisphenol A disrupts pancreatic beta-cell function in vivo and induces insulin resistance. *Environ Health Perspect* **114**, 106-112 (2006).
28. S. Soriano *et al.*, Rapid insulinotropic action of low doses of bisphenol-A on mouse and human islets of Langerhans: role of estrogen receptor beta. *PLoS One* **7**, e31109 (2012).
29. E. Leighton, C. A. Sainsbury, G. C. Jones, A Practical Review of C-Peptide Testing in Diabetes. *Diabetes Ther* **8**, 475-487 (2017).
30. R. L. Rich *et al.*, Kinetic analysis of estrogen receptor/ligand interactions. *Proc Natl Acad Sci U S A* **99**, 8562-8567 (2002).
31. J. Corzo, Time, the forgotten dimension of ligand binding teaching. *Biochem Mol Biol Educ* **34**, 413-416 (2006).
32. B. Knierim, K. P. Hofmann, O. P. Ernst, W. L. Hubbell, Sequence of late molecular events in the activation of rhodopsin. *Proc Natl Acad Sci U S A* **104**, 20290-20295 (2007).
33. C. K. Meyer *et al.*, Signaling states of rhodopsin. Retinal provides a scaffold for activating proton transfer switches. *J Biol Chem* **275**, 19713-19718 (2000).
34. A. Scheer, F. Fanelli, T. Costa, P. G. De Benedetti, S. Cotecchia, The activation process of the alpha1B-adrenergic receptor: potential role of protonation and hydrophobicity of a highly conserved aspartate. *Proc Natl Acad Sci U S A* **94**, 808-813 (1997).
35. W. A. Timms D, Kelly DR, Broadley KJ, Davies RH Ligand-activated trans-membrane proton transfer in beta 1-adrenergic and m2-muscarinic receptors. *Recept Channels* **2**, 107-119 (1994).
36. Y. Mizuno, K. Katayama, H. Imai, H. Kandori, Early Proton Transfer Reaction in a Primate Blue-Sensitive Visual Pigment. *Biochemistry* **61**, 2698-2708 (2022).
37. A. P. Demchenko, Proton transfer reactions: From photochemistry to biochemistry and bioenergetics. *BBA Adv* **3**, 100085 (2023).
38. F. Acconcia, V. Pallottini, M. Marino, Molecular Mechanisms of Action of BPA. *Dose Response* **13**, 1559325815610582 (2015).

39. A. Nadal *et al.*, Extranuclear-initiated estrogenic actions of endocrine disrupting chemicals: Is there toxicology beyond paracelsus? *J Steroid Biochem Mol Biol* **176**, 16-22 (2018).
40. G. Nassa *et al.*, A large set of estrogen receptor beta-interacting proteins identified by tandem affinity purification in hormone-responsive human breast cancer cell nuclei. *Proteomics* **11**, 159-165 (2011).
41. C. Stellato *et al.*, Identification of cytoplasmic proteins interacting with unliganded estrogen receptor alpha and beta in human breast cancer cells. *Proteomics* **15**, 1801-1807 (2015).
42. P. Alonso-Magdalena, I. Quesada, A. Nadal, Endocrine disruptors in the etiology of type 2 diabetes mellitus. *Nat Rev Endocrinol* **7**, 346-353 (2011).
43. A. Nadal, I. Quesada, E. Tuduri, R. Nogueiras, P. Alonso-Magdalena, Endocrine-disrupting chemicals and the regulation of energy balance. *Nat Rev Endocrinol* **13**, 536-546 (2017).
44. R. S. Dos Santos, R. M. Medina-Gali, I. Babiloni-Chust, L. Marroqui, A. Nadal, In Vitro Assays to Identify Metabolism-Disrupting Chemicals with Diabetogenic Activity in a Human Pancreatic beta-Cell Model. *Int J Mol Sci* **23**, (2022).
45. A. Nadal, B. Soria, Glucose metabolism regulates cytosolic Ca2+ in the pancreatic beta-cell by three different mechanisms. *Adv Exp Med Biol* **426**, 235-243 (1997).
46. M. Valdeolmillos, A. Nadal, D. Contreras, B. Soria, The relationship between glucose-induced K+ATP channel closure and the rise in [Ca2+]i in single mouse pancreatic beta-cells. *J Physiol* **455**, 173-186 (1992).
47. W. Thangnipon *et al.*, Protective role of N-trans-feruloyltyramine against beta-amyloid peptide-induced neurotoxicity in rat cultured cortical neurons. *Neurosci Lett* **513**, 229-232 (2012).
48. A. Liu *et al.*, High-performance thin-layer chromatography coupled with HPLC-DAD/HPLC-MS/MS for simultaneous determination of bisphenol A and nine brominated analogs in biological samples. *Anal Bioanal Chem* **411**, 725-734 (2019).
49. A. J. M. M. Gregory R. Fulmer, Nathaniel H. Sherden, Hugo E. Gottlieb, Abraham Nudelman, Brian M. Stoltz, John E. Bercaw, and Karen I. Goldberg, NMR Chemical Shifts of Trace Impurities: Common Laboratory Solvents, Organics, and Gases in Deuterated Solvents Relevant to the Organometallic Chemist. *Organometallics* **29**, 2176–2179 (2010).
50. A. A. Perez-Serna *et al.*, BCL-XL Overexpression Protects Pancreatic beta-Cells against Cytokine- and Palmitate-Induced Apoptosis. *Int J Mol Sci* **24**, (2023).
51. J. Martinez-Pinna *et al.*, Oestrogen receptor beta mediates the actions of bisphenol-A on ion channel expression in mouse pancreatic beta cells. *Diabetologia* **62**, 1667-1680 (2019).
52. I. Santin, R. S. Dos Santos, D. L. Eizirik, Pancreatic Beta Cell Survival and Signaling Pathways: Effects of Type 1 Diabetes-Associated Genetic Variants. *Methods Mol Biol* **1433**, 21-54 (2016).
53. S. Ciordia *et al.*, Digging deeper into bile proteome. *J Proteomics* **230**, 103984 (2021).
54. G. Bindea *et al.*, ClueGO: a Cytoscape plug-in to decipher functionally grouped gene ontology and pathway annotation networks. *Bioinformatics* **25**, 1091-1093 (2009).
55. G. Bindea, J. Galon, B. Mlecnik, CluePedia Cytoscape plugin: pathway insights using integrated experimental and in silico data. *Bioinformatics* **29**, 661-663 (2013).
56. T. Metsalu, J. Vilo, ClustVis: a web tool for visualizing clustering of multivariate data using Principal Component Analysis and heatmap. *Nucleic Acids Res* **43**, W566-570 (2015).
57. M. Biasini *et al.*, SWISS-MODEL: modelling protein tertiary and quaternary structure using evolutionary information. *Nucleic Acids Res* **42**, W252-258 (2014).

58. S. Salentin, S. Schreiber, V. J. Haupt, M. F. Adasme, M. Schroeder, PLIP: fully automated protein-ligand interaction profiler. *Nucleic Acids Res* **43**, W443-447 (2015).
59. A. Dobin *et al.*, STAR: ultrafast universal RNA-seq aligner. *Bioinformatics* **29**, 15-21 (2012).
60. R. Patro, G. Duggal, M. I. Love, R. A. Irizarry, C. Kingsford, Salmon provides fast and bias-aware quantification of transcript expression. *Nature Methods* **14**, 417-419 (2017).
61. M. I. Love *et al.*, Tximeta: Reference sequence checksums for provenance identification in RNA-seq. *PLOS Computational Biology* **16**, e1007664 (2020).
62. M. I. Love, W. Huber, S. Anders, Moderated estimation of fold change and dispersion for RNA-seq data with DESeq2. *Genome Biology* **15**, 550 (2014).
63. J. T. Leek, svaseq: removing batch effects and other unwanted noise from sequencing data. *Nucleic Acids Research* **42**, e161-e161 (2014).

Acknowledgments:

The authors thank Beatriz Bonmati Botella, Maria Luisa Navarro, and Salomé Ramon for their excellent technical assistance. We thank Dr. J.A. Encinar (IDiBE-UMH) for docking simulations. Workflow schemes in figures 4 and 5 were performed with BioRender.

Funding

This work was supported by:

Ministerio de Ciencia e Innovación, Agencia Estatal de Investigación (AEI) grant PID2020-117294RB-I00 (AN, JM-P), PID2020-117569RA-I00 and CNS2022-135505 (LM), PID2020-113112RB-100 (PA-M).

Generalitat Valenciana PROMETEO II/2020/006 (AN).

European Union's Horizon 2020 research and innovation programme under grant agreement GOLIATH No. 825489 (AN, PB).

RSdS holds a Miguel Servet Program from Instituto de Salud Carlos III CP23/00026. CIBERDEM is an initiative of the Instituto de Salud Carlos III.

Author contributions

AN: conceived the study, designed experiments, acquired funds, and oversaw the project. JM-P, PB acquired funds, designed and performed experiments and analyzed data. RM-G, RSDS, PA-M, MS-M, RS-N, SS, GF-P, LP, RM, SC, MG, LM designed and

performed experiments and analyzed data. AN. wrote the manuscript. All authors participated in reviewing and editing the manuscript.

Competing interests

Authors declare that they have no competing interests.

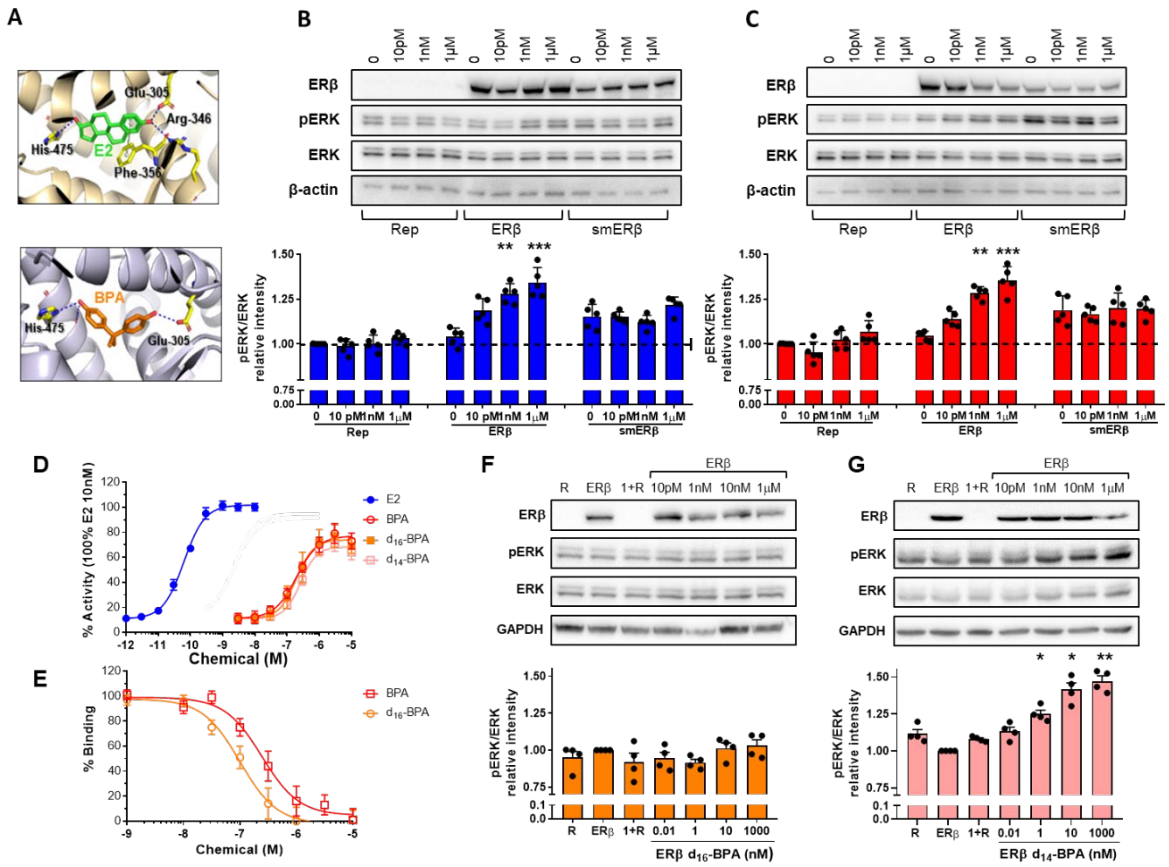

Fig. 1. Activation of the extra-nuclear pathway in HEK293 cells transfected with ERβ.

(**A**) Interaction of E2 (upper panel) with Glu^{305}, Arg^{346} and His^{475}, and of BPA (lower panel) with Glu^{305} and His^{475} within the ligand binding site of ERβ. Amino acids involved in H-bonds are marked with a blue dashed line. (**B** and **C**) HEK293 cells transfected with the reporter plasmid (Rep), ERβ or the ERβ single mutant (smERβ) were treated with E2 in B or BPA in C, at the indicated concentrations for 1 hour. Top part shows representative immunoblots of ERβ, pERK, ERK, and β-actin expression. Activation values of pERK were quantified against ERK and are shown as graphs (low). (**D**) Luciferase assay in HELN ERβ reporter cells. Cells were treated with E2, BPA, d_{16}-BPA and d_{14}-BPA for 16 hours at the indicated concentrations. The maximal luciferase activity (100%) was obtained with 10 nM E2. Data are represented as the percentage of maximal E2 induction. Values are the mean±SEM from 3 separated experiments. (**E**) Competitive inhibition of [^{3}H]-E2 binding to hERβ by BPA and d_{16}-BPA. HELN ERβ cells were incubated with different concentrations of BPA and d_{16}-BPA in the presence of 0.1 nM E2 [^{3}H]-E2 during 16 hours. Data are represented as the percentage of maximal [^{3}H]-E2 binding. Values are the mean±SEM from 3 separated experiments. (**F** and **G**) HEK293 cells transfected with reporter plasmid labeled as R, or ERβ were treated with d_{16}-BPA or d_{14}-BPA at the indicated concentrations for 1 hour. Top part shows

representative immunoblot of ERβ expression, pERK, ERK and GAPDH. ERK phosphorylation was quantified against total ERK (low). Data are shown as mean±SEM of 4 separated experiments. *P < 0.05, **P < 0.01, ***P < 0.001. One way ANOVA followed by Tukey test. Note that the column labelled as ERβ represents cells transfected with ERβ plus 0.00002% DMSO used as a control.

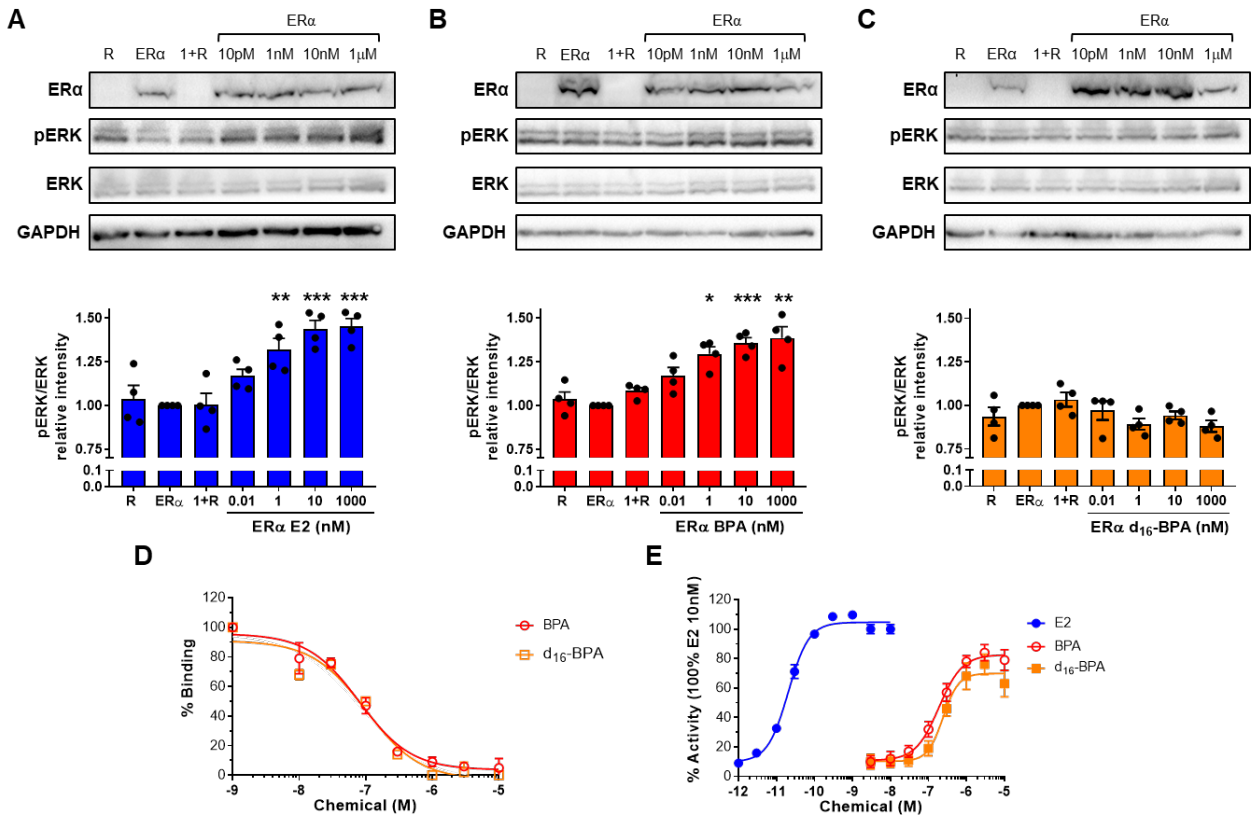

Fig.2. ERK activation in HEK293 cells transfected with ERα.

(**A-C**) Representative immunoblots of ERα, pERK, ERK and GAPDH (top), and quantification of pERK versus ERK (bottom) in response to vehicle (DMSO, indicated as ERα), E2, BPA and d_{16}-BPA for 1 hour in HEK293 cells transfected with either reporter (Rep or R) or ERα plasmids. Results are expressed as mean±SEM from 4 separated experiments. *P < 0.05, **P < 0.01, ***P < 0.001, One-way ANOVA followed by Tukey test. (**D**) Luciferase assay in HELN ERα reporter cells. Cells were treated with E2, BPA and d_{16}-BPA for 16 hours at the indicated concentrations. The maximal luciferase activity (100%) was obtained with 10 nM E2. Data are represented as the percentage of maximal E2 induction. Values are the mean±SEM from 3 separated experiments. (**E**) Competitive inhibition of [^{3}H]-E2 binding to hERα by BPA and d_{16}-BPA. HELN ERα cells were incubated with different concentrations of BPA and d_{16}-BPA in the presence of 0.1nM E2 [^{3}H]-E2 during 16 hours. Data are represented as the percentage of maximal [^{3}H]-E2 binding. Values are the mean±SEM from 3 separated experiments.

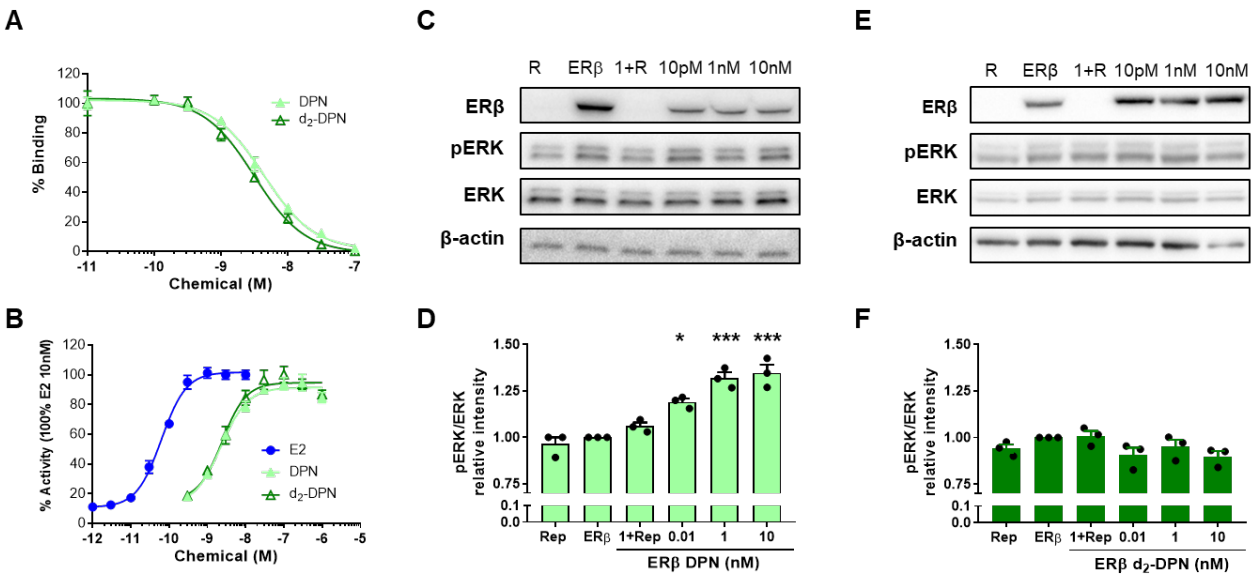

Fig. 3. Effect of DPN in the ERK activation in HEK293 cells transfected with ERβ.

(**A**) Competitive inhibition of [^{3}H]-E2 binding to hERβ by DPN and d_2-DPN. HELN ERβ cells were incubated with different concentrations of DPN and d_2-DPN in the presence of 0.1nM nM E2 [^{3}H]-E2 during 16 hours. Values are represented as mean±SEM from 3 separated experiments. (**B**) Luciferase assay in HELN ERβ reporter cells. Cells were treated with E2, DPN and d_2-DPN for 16 hours at the indicated concentrations. The maximal luciferase activity (100%) was obtained with 10 nM E2. Data are represented as the percentage of maximal E2 induction. Values are the mean±SEM from 3 separated experiments. (**C** and **D**) HEK293 cells were transfected with reporter (R) or ERβ plasmid and treated with DPN at 10pM, 1nM, 10nM and 1µM concentrations for 1 hour. Representative immunoblots are shown of ERβ, ERK and β-actin expression as well as pERK phosphorylation. In the low part, graphs showing the quantification of pERK expressed as the ratio pERK/ERK relative intensity. (**E** and **F**) The same as in C and D but treating the cells with d_2-DPN. *P < 0.05, **P < 0.01, ***P < 0.001, One-way ANOVA followed by Tukey test, n=3 separated experiments.

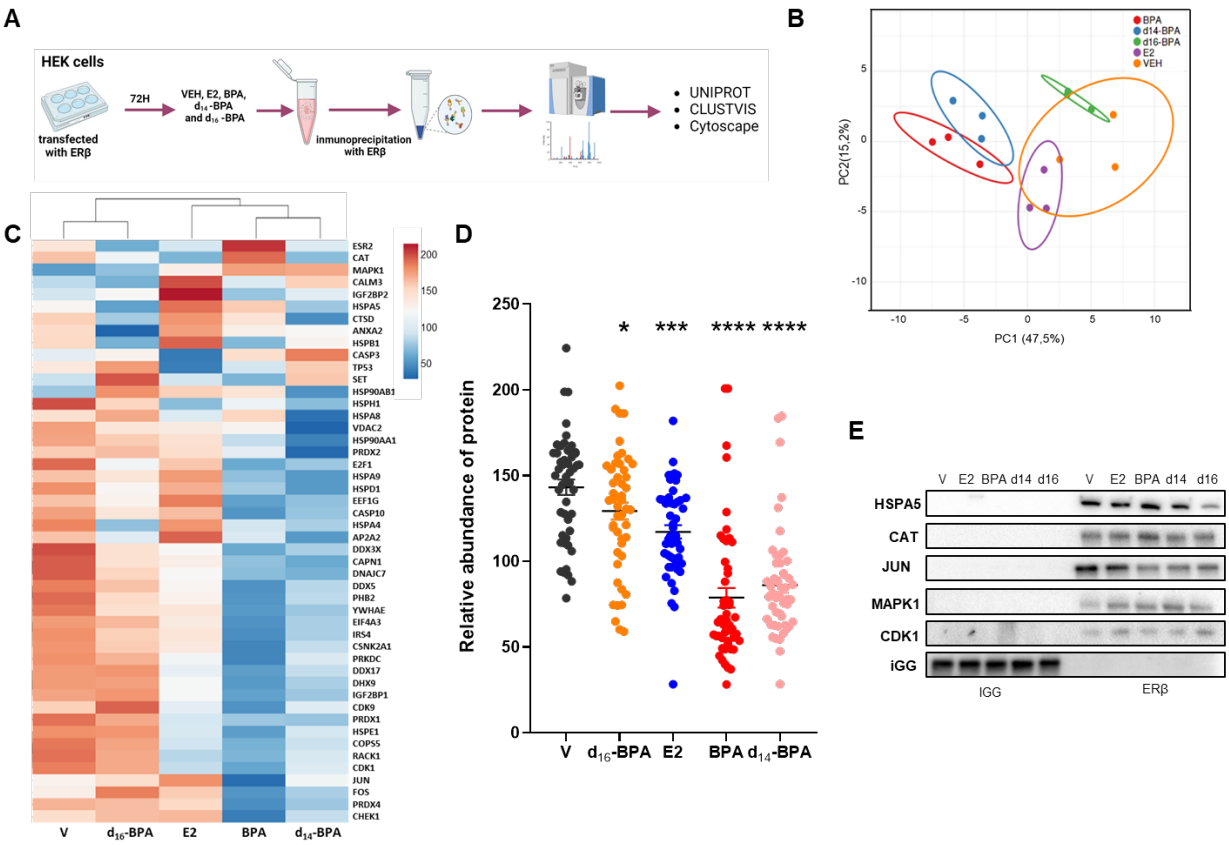

Figure 4. Changes in the ERβ interactome in response to E2, BPA, d_{14}-BPA and d_{16}-BPA.

(**A**) Summary of the experimental workflow applied to identify ERβ-interacting proteins: ERβ-transfected HEK293 cells were subjected to different treatments, vehicle (0.00002% DMSO, indicated as V), E2, BPA, d_{14}-BPA and d_{16}-BPA at a concentration of 1 nM for 1 hour, and then immunoprecipitated with an anti-ERβ antibody, to identify ERβ-interacting proteins by proteomics. (**B**) Principal component plot (PCA) of ERβ interactome assessment in ERβ-transfected HEK293 cells treated with V, E2, BPA, d_{14}-BPA and d_{16}-BPA for 1 hour. Graph was developed using relative abundances of proteins identified by proteomics. (**C**) Heat map of molecular signatures showing the relative abundance of 49 proteins directly linked to ERβ. The heatmap data matrix visualizes the values in the cells using a color gradient that gives an overview of the largest and smallest values in the matrix. The cluster lines at the top show the grouping by treatment. (**D**) Graph of relative protein abundances showing the independent behavior of each treatment. One-way ANOVA followed by Dunn test was performed showing significant differences between groups, *$P < 0.05$, ***$P < 0.001$, ****$P < 0.0001$. (**E**) Immunoblots of representative proteins interacting with ERβ. The proteins were evaluated in immunoprecipitates of IGG or with ERβ, in the different treatments performed (V, E2, BPA d_{14}-BPA and d_{16}-BPA) for 1 hour.

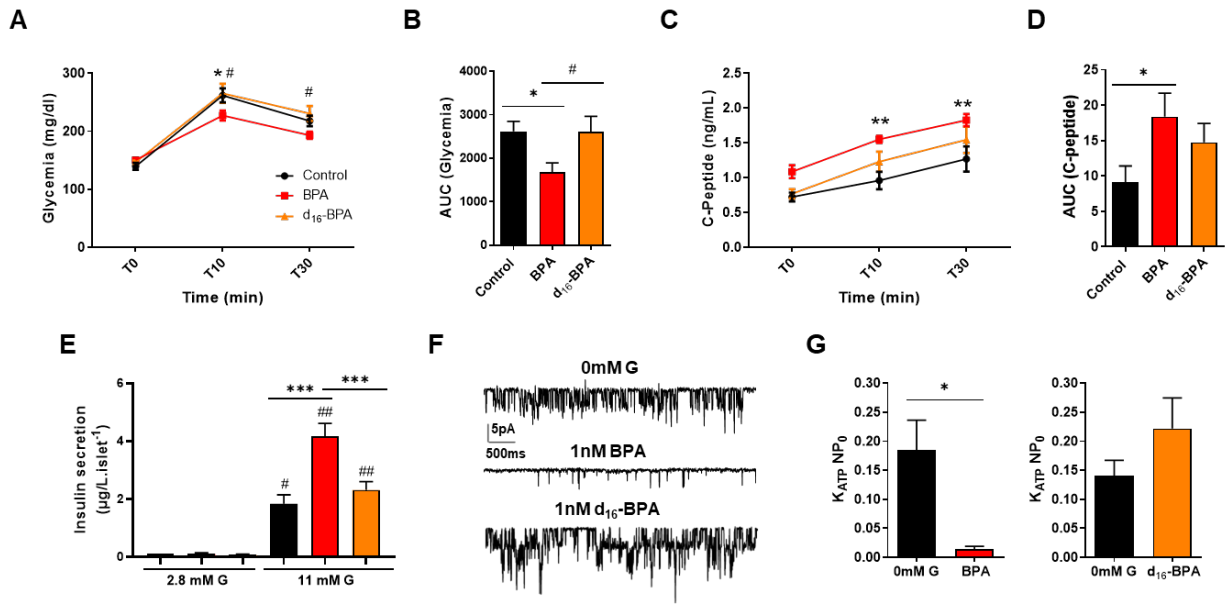

Figure 5. Rapid actions of BPA and d_{16}-BPA on pancreatic β-cells.

(**A**) Glucose levels (mg/dL) and (**B**) area under the curve (AUC), during a intraperitoneal glucose tolerance test in response to a glucose load of 1.5 g/kg body weight after a 6-hour fast and an acute injection of vehicle (Control), BPA, or d_{16}-BPA (both at 10µg/kg) (n = 9-10 mice/group). Data are shown as mean ± SEM. (**C**) Plasma C-peptide levels and (**D**) area under the curve, during the same experiment as (A-B) (n=9 mice/group). Data are shown as mean ± SEM. *P < 0.05, **P < 0.01 (control vs BPA), #P < 0.05 (BPA vs d_{16}-BPA), Two-way ANOVA followed by Tukey test (A and C) and one-way ANOVA (B and D) followed by Tukey or Bonferroni test. (**E**) Insulin secretion was measured at 2.8 and 11 mM glucose (G) in islets from C57BL/6 J mice. After a 2-hour starvation period, vehicle, 1 nM BPA, or 1 nM d_{16}-BPA was added to each glucose solution so that islets remained under treatment throughout the entire assay (1-hour exposure). Insulin release was measured by ELISA. Data are shown as means ± SEM (n = 5 independent islet preparations). # P < 0.05 and ## P ≤ 0.01 *vs* its respective treatment. *** P < 0.001. Two-way ANOVA plus Sidak's tests. (**F**) Representative recordings of K_{ATP} channel activity in 0 mM glucose (up), 10 min after application of 1nM BPA (middle) or 1nM d_{16}-BPA (down). (**G**) Average mean open probability of K_{ATP} channels elicited by 0 mM glucose and in the presence of 1nM BPA (left, n = 8 cells) or 1nM d_{16}-BPA (right, n= 8 cells). * P<0.05, paired t-test.

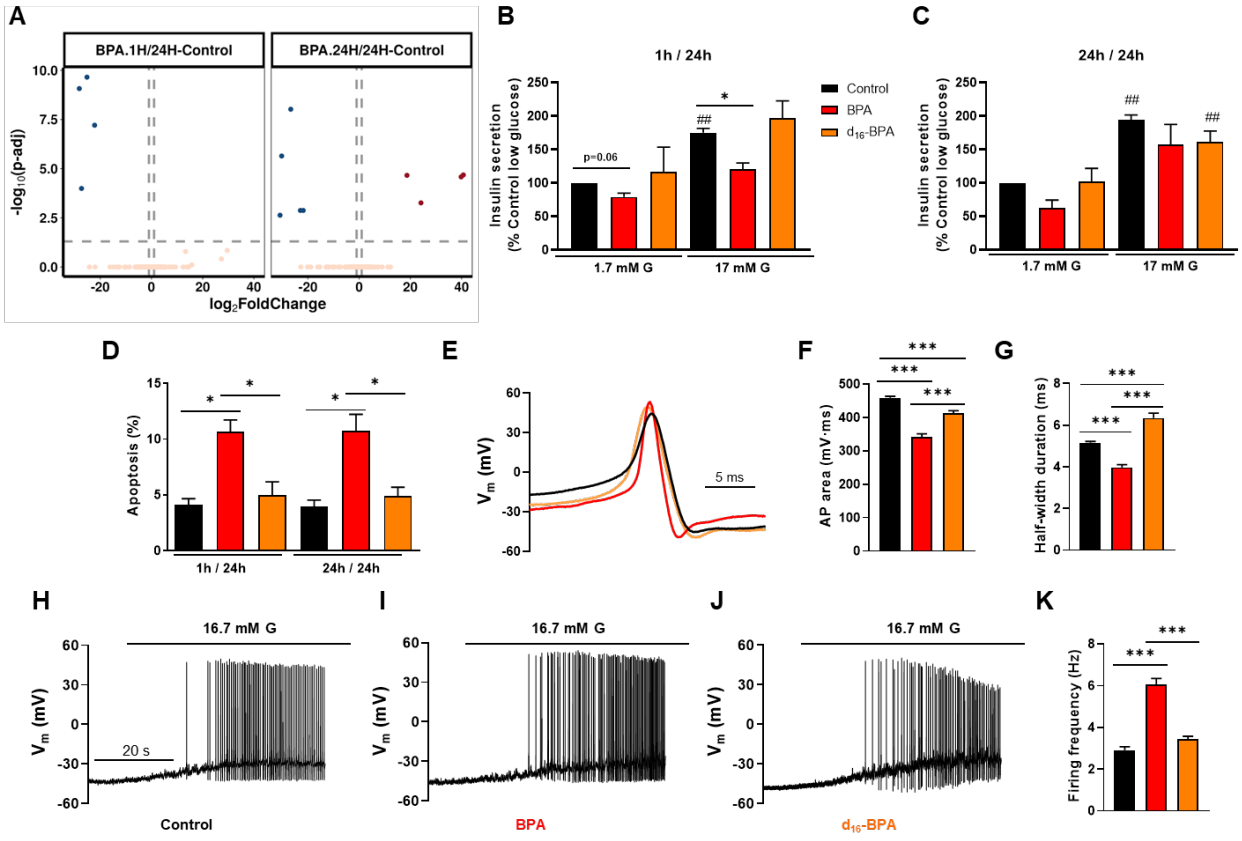

Figure 6. Long-term consequences of acute treatment with BPA and d_{16}-BPA in INS-1E cells.

(**A**) Volcano plots illustrating the differential expression of genes in cells treated for 1h and 24h with 1nM BPA compared to control cells (measured in both cases at 24h). Dotted lines indicate significance thresholds for significance (|log2 fold change| > 1 and adjusted P < 0.05). Red, upregulated genes; blue, downregulated genes; peach, stable genes. (**B and C**) Insulin secretion in INS-1E cells treated with vehicle, 1 nM BPA or 1 nM d_{16}-BPA for 1 h (**B**) or 24 h (**C**). GIIS was measured at 1.7 or 17 mM glucose (G) for 30 minutes. Data are normalized to insulin secretion at low glucose (i.e., 1.7 mM G) in vehicle-treated cells (considered as 100%). Data are shown as means ± SEM (n = 4 independent experiments). ## P ≤ 0.01 *vs* its respective treatment. *P < 0.05. Two-way ANOVA plus Dunnett's or Sidak's tests. (**D**) Apoptosis evaluated using Hoechst 33342 and propidium iodide staining in INS-1E cells treated with vehicle, 1 nM BPA or 1 nM d_{16}-BPA for 1 h (left) or 24 h (right). In both cases, apoptosis was assessed after 24 h. Data are shown as means ± SEM (n = 4 independent experiments). **P<0.01 (control vs BPA), One way ANOVA followed by Dunnett's test. (**E**) Superimposed representative action potentials at 16.7 mM glucose in control, 1nM BPA or 1nM d_{16}-BPA during 1h and measuring at 24h. (**F**) Average area under the action potential and (**G**) action

potential half-width duration at 16.7 mM glucose (197, 279 and 214 action potentials in the control, 1 nM BPA, and 1 nM d_{16}-BPA respectively; *n* = 6, 5, and 5 cells). ***P<0.001, One way ANOVA followed by Tukey test. (**H**, **I**, **J**) Representative action potential firing in response to 16,7 mM glucose in the presence of vehicle (H), 1 nM BPA (I), and 1 nM d_{16}-BPA (J). (**K**) Average action potential firing frequency at 16.7 mM glucose (191, 272 and 209 action potentials in the control, 1 nM BPA, and 1 nM d_{16}-BPA respectively; n = 6, 5, and 5 cells). ***P<0.001, One way ANOVA followed by Tukey test.